HHS Public Access

Author manuscript

Biomech Model Mechanobiol. Author manuscript; available in PMC 2019 February 01.

Published in final edited form as:

Biomech Model Mechanobiol. 2018 February ; 17(1): 159–168. doi:10.1007/s10237-017-0951-1.

The Potential for Intercellular Mechanical Interaction – Simulations of Single Chondrocyte Versus Anatomically Based Distribution

Jason P. Halloran[1], **Scott C. Sibole**[2], and **Ahmet Erdemir**[3]

[1]Department of Mechanical Engineering and the Mechanics and Control of Living Systems Lab, Cleveland State University, Cleveland, Ohio, USA

[2]Department of Biomedical Engineering, Human Performance Lab, University of Calgary, Calgary, Alberta, CANADA

[3]Computational Biomodeling (CoBi) Core and the Department of Biomedical Engineering, Lerner Research Institute, Cleveland Clinic, Cleveland, Ohio, USA

Abstract

Computational studies of chondrocyte mechanics, and cell mechanics in general, have typically been performed using single cell models embedded in an extracellular matrix (ECM) construct. The assumption of a single cell microstructural model may not capture intercellular interactions or accurately reflect the macro-scale mechanics of cartilage when higher cell concentrations are considered, as may be the case in many instances. Hence, the goal of this study was to compare cell level response of single and eleven cell biphasic finite element (FE) models, where the latter provided an anatomically based cellular distribution representative of the actual number of cells for a commonly used 100 μm edge cubic representative volume in the middle zone of cartilage. Single cell representations incorporated a centered single cell model and eleven location corrected single cell models; the latter to delineate the role of cell placement in the representative volume element. A stress relaxation test at 10% compressive strain was adopted for all simulations. During transient response, volume averaged chondrocyte mechanics demonstrated marked differences (up to 60% and typically greater than 10%) for the centered single versus the eleven cell models, yet steady-state loading was similar. Cell location played a marked role, due to inhomogeneity of the displacement and fluid pressure fields at the macroscopic scale. When the single cell representation was corrected for cell location, the transient response was consistent while steady-state differences on the order of 1–4% were realized, which may be attributed to intercellular

Corresponding Author: Jason Halloran, PhD, Department of Mechanical Engineering, Cleveland State University, phone: +1 (216) 687 4662, j.halloran64@csuohio.edu.

7. Dissemination

A download package incorporating the embedded and autonomous models, postprocessing scripts, and simulation results is freely accessible in the Downloads section of the project web site https://simtk.org/home/j2c.

Compliance with Ethical Standards:

Funding was provided by the National Institute of Biomedical Imaging and Bioengineering, National Institutes of Health (R01EB009643: Erdemir, Principal Investigator)

Conflict of Interest: Author Halloran has received research grants from Active Implants Inc, Orthosensor Inc. and Stryker Orthopaedics. Author Erdemir has received research grants from the National Aeronautics and Space Administration (NASA). Author Erdemir is a lead member of the Committee on Credible Practice of Modeling & Simulation in Healthcare.

mechanical interactions. Anatomical representations of the superficial and deep zones, where cells reside in close proximity, may exhibit greater intercellular interactions, but these have yet to be explored.

Keywords

multiscale; computational modeling; finite element; cartilage; chondrocyte; poroelastic; biphasic; tissue mechanics; cell mechanics; homogenization

2. Introduction

Among many other factors, including genetic, environmental and soluble mediators, mechanical loading influences articular cartilage maintenance through the balance of growth and degradation [1]. Within the cartilage, the mechanical environment of chondrocytes, the sole resident cell type, has been shown to be a contributor to cellular activity and, in turn, tissue health. The surrounding microstructural and multi-physical nature of cartilage dictate cellular loading, with demonstrated depth- and location-dependent differences [2], [3]. Chondrocyte density, including shape and arrangement, and collagen fiber orientation have been shown to vary across stages of development, physical locations on the articular surface, and species [4], [5]. Within a given region, the extracellular microstructure, the pericellular and cellular regions, and the surrounding fluid, nearly-immobile proteoglycan molecules, and mobile ions interact to dictate the biomechanical response of the chondrocytes [1].

Experimental modalities have been vital to understand the mechanics of cartilage as well as the underlying chondrocyte mechanobiological response. Joint level load sharing and the functional response of cartilage has been studied, with cartilage playing an integral role at this spatial scale [6], [7]. These multiscale chondrocyte mechanics have been investigated through laser scanning microscopy coupled to mechanical testing systems *in situ* [8]–[10] and *in vivo* [11]. Additional measures of chondrocyte mechanobiology have been inferred through the observation of calcium signalling in response to tissue-level applied mechanics [12], [13]. With regards to material behavior, basic mechanical properties have been quantified and provide context to the micro-mechanical and chemical environment of the cells [14], [15]. As they provide controlled conditions, tissue explant samples, whether acquired from biological sources or engineered constructs, have offered much of the available information on chondrocyte mechanical response [16].

Computational simulations of chondrocyte mechanics have provided both information complimentary to experimentation, detailing the underlying mechanics, and an avenue to investigate fundamental aspects of cartilage and chondrocyte mechanics that are infeasible to capture experimentally [3], [7], [17]. Simulation offers a unique mechanical evaluation strategy utilizing metrics such as the local stress, strain, fluid flow, and pressure. Often hypothesis-driven and at times performed in a parametric fashion, such studies have looked at cell deformation within the context of the tissue microstructure [18]. In particular, depth dependent simulations including singular or combined mechanics of the collagen fibrillar network (extracellular matrix, ECM), pericellular matrix, and chondrocytes have been developed [19], [20]. Especially when the influence of the surrounding aqueous solution is

included, as accounted for through biphasic theory [21], such studies have highlighted the potential for complex, time dependent loading of chondrocytes [3], [17], [22].

In previous chondrocyte simulation studies, representation of the cells within a neighboring volume were limited to a single cell embedded in an cubic ECM volume, commonly with an edge size of 100 μm [17], [18]. Typically, deformations predicted from a homogeneous tissue model were used to drive such simulations. Implicit in this setup are: i) the assumption of the equivalence of macrostructural (tissue) constitutive response and average stress-strain response of the microstructural (cellular) model, ii) the ability of simplified data passing approaches from the macro- to cell-scales to reflect embedded cell response, iii) the cell representation in extracellular matrix, which commonly relies on the model of a single, centered cell within in the micro-scale geometric representation of the extracellular matrix, and iv) the neglection of mechanical interaction between cells. To overcome assumption i, this study adopted an embedded model, where the representative volume element (RVE) was directly modeled within a homogeneous ECM construct. Likewise, circumventing assumption ii an embedded model eliminates the need for a data passing approach. Recent work highlighted important considerations for data passing when a post-processing approach is used for prediction of chondrocyte mechanics [23]. This study found that if metrics other than cellular aspect ratio are of interest, higher order data passing schemes or direct coupling of micro- and macrostructural models, as was performed in this study, should be considered. Regarding assumption iii, while computational models of single cells have provided invaluable insight into the chondrocyte mechanical environment, articular cartilage, especially at early stages of development and for certain zonal regions, can exhibit much higher cell concentrations than previously assumed [5]. The predictions of chondrocyte mechanics as obtained from a single cell assumption may not be adequate for cartilage with high chondrocyte density, due to misrepresentation of the true volume fraction of the cells in the ECM (assumption iii) and the potential to overlook cellular interactions (assumption iv). Hence, the goal of this study was to compare the mechanical response of chondrocytes in single and physiologically based eleven cell [5] biphasic finite element (FE) models. The driving questions behind this goal are whether potential intercellular mechanical interactions can be delineated and whether the mechanics of cells change as a result of neighboring cells.

3. Methods

3.1 Models

A 100x100x100 μm^3, the commonly assumed RVE, cell-scale finite element model was embedded in a 1x1x1 mm^3 (tissue-scale) hexahedral mesh construct, which approximated a layer of cartilage in the middle or transitional zone (Figure 1). All models were meshed with linear hexahedral elements using TrueGrid (XYZ Scientific Applications, Inc., Livermore, CA). In following, relevant features of the model are summarized. For a more detailed description, the reader is encouraged to refer to Sibole et al., 2013 [23].

For the RVE, two general cases were considered: a single (centered) cell and an eleven cell randomly distributed configuration (Figure 1). For the given RVE size, eleven cells represent an anatomically based volume fraction of cells in mature human cartilage [5]. During random placement, minimum pericellular-to-pericellular and pericellular-to-tissue-edge

spacing was enforced at 2.5 μm and 1.25 μm, respectively[24]. The cells had radii of 5 μm and were surrounded by a layer of pericellular matrix with a thickness of 2.5 μm [25].

A biphasic constitutive model was utilized, with a nonlinear elastic (Neo-Hookean) solid component and the fluid component modeled with Darcy's Law with strain invariant permeability [26]. FEBio version 1.5.0 was used as the simulation software [20] where in a biphasic analysis the Cauchy stress was defined as:

$$\boldsymbol{T} = -p\boldsymbol{I} + \boldsymbol{T}^{\boldsymbol{e}} \quad (1)$$

where p is the interstitial fluid pressure and $\boldsymbol{T}^{\boldsymbol{e}}$ is the stress from the porous Neo-Hookean elastic matrix material. The Neo-Hookean material was implemented in FEBio using the following strain energy function:

$$W = \frac{\mu}{2}(I_1 - 3) - \mu \ln J + \frac{\lambda}{2}(\ln J)^2 \quad (2)$$

where I_1 is the first invariant of the right Cauchy-Green deformation tensor, J is the determinant of the deformation gradient tensor, and μ and λ are material coefficients that are related to the Young's modulus and Poisson ratio [20]. Darcy's law was used to relate the hydraulic permeability, $\boldsymbol{k}$, to the volumetric flux, $\boldsymbol{w}$, of the fluid relative to the solid,

$$\boldsymbol{w} = -\boldsymbol{k} \cdot \nabla p \quad (3)$$

where $\boldsymbol{k}$ did not vary as a function of strain. The mixture momentum balance for quasi-static conditions (no external body forces),

$$div\boldsymbol{T} = -\nabla p + div\boldsymbol{T}^{\boldsymbol{e}} = 0, \quad (4)$$

and the mixture mass balance,

$$div(\boldsymbol{v}^{\boldsymbol{s}} + \boldsymbol{w}) = 0 \quad (5)$$

defined the governing equations. Note that $\boldsymbol{v}^{\boldsymbol{s}}$ was the solid velocity and div was the divergence. Additional detail on the material model can be found in the FEBio user's manual. For the described biphasic material, constitutive parameter values were adopted from [25] for the middle zone cartilage depth. The extracellular matrix had a Young's modulus of 1.0 MPa, a Poisson's ratio of 0.125, and a hydraulic permeability of 0.002 mm^4/N-s. For the pericellular matrix these were 0.043 MPa, 0.125, and 0.002 mm^4/N-s and

for the cell(s), 0.001 MPa, 0.4, and 0.001 mm^4/N-s. The larger block, in which the single cell and eleven cell RVEs were embedded, was given the same properties as the ECM.

The interface between the RVE and the tissue-scale models contained hexahedral transition elements, which allowed for node-to-node merging of the two meshes and a more coarse mesh for the tissue scale model, and eliminated the need for enforcement of any coupling constraint, i.e., a data passing regime [23]. The embedded models contained 147,768 and 152,868 elements for single cell and eleven cell cases, respectively. In the tissue-scale region of the models the approximate average element edge length was 3 μm, while the elements in the embedded RVEs had edge lengths of approximately 0.2 μm. A mesh convergence study was not conducted for the multi-scale construct models as these were near the upper bound of the available shared memory architecture computational resources. However, a mesh convergence study was previously conducted on the single cell RVE model. Models of lower mesh density (25,889 elements) than those employed in this were shown to converge in 3rd principal stress, strain, and total fluid flux for the single cell case [24]. Due to the need to satisfy strict element density ratios at the transition interfaces, the converged meshes had their element densities further refined, but since the meshes were of higher density, these were also assumed to be converged.

The tissue-cell scale constructs were subjected to 10% nominal compressive strain (−0.1 mm), ramped over 0.1 seconds and held constant for an additional 99.9 seconds. Confined compression boundary conditions were defined, which allowed for zero expansion and fluid flux normal to the lateral faces. For the top and bottom surfaces, two fluid drainage cases were considered: Case A) zero fluid pressure boundary conditions, which allowed free-draining of fluid, were prescribed to both the top and bottom faces; and Case B) zero fluid pressure was prescribed for only the top face and the bottom face was non-draining. Simulations were conducted for compressive strain in a single direction, for both cases A and B.

While comparison of the 11 and single cell simulation results offered a means to observe mechanical differences, the cause of those differences may be due to multiple factors, namely, cell position and intercellular mechanical influence. To understand the potential for position dependence, additional simulations were conducted where the material assignments of the 11 cell model were adjusted such that only one chondron (the chondrocyte and its surrounding pericellular matrix) at a time was represented, by replacing all other chondron materials with ECM. This was performed for each of the 11 cells and both Case A and B boundary conditions, resulting in a total of 22 simulations. The results for each of the location specific single chondrocyte simulations could then be compared to the corresponding chondrocyte in the 11 cell simulation. With this method, the position of the cell is the same in both scenarios, but intercellular mechanical influence could only occur in the 11 cell simulations. To summarize and delineate the results, for both Case A and B boundary conditions, the simulations consisted of centered single cell (CSC), eleven cell randomly distributed (EC), and a series of 11 location corrected single cell (LCSC) analyses. A custom Python script was used to post-process FEBio version 1.5.0 [26] result files for chondrocyte mechanical metrics: volume-averaged effective stress and strain, volume-averaged maximum shear strain, volumetric strain, net mass exchange rate, and change in

aspect ratio. These were calculated as outlined in a previous study [23]. For visual representation, cell metrics were plotted throughout the simulations. To provide quantitative comparison, percent differences as a function of time were calculated between 1.) the CSC and each cell in the EC simulation and 2.) the LCSC results and the corresponding cell in the EC simulation using the following:

$$\%\ Difference(m,i,t) = \frac{Cell_i(m,t) - EC_i(m,t)}{EC_i(m,t)} * 100 \quad (6)$$

where m is a given mechanical metric (outlined above), t is time, $Cell_i$ is a given cell ($i = 1$ to 11 for the LCSC and $i = 1$ for the CSC results), and EC_i are each of the eleven cells in the EC simulation (i = 1 to 11). Finally, to further understand the potential for cellular mechanical interaction, root mean square (RMS) values for all metrics throughout the cycle were calculated between the EC and LCSC results using:

$$RMS(m,i) = \frac{\sqrt{\frac{1}{n}\sum_{t=0}^{n}\left(Cell_i(m,t) - EC_i(m,t)\right)^2}}{\left|max\left(EC_i(m,t)\right) - min\left(EC_i(m,t)\right)\right|} \quad (7)$$

where t was discretized into $n = 30$ data points throughout the loading cycle [23].

Due to the high computational cost of the large degree of freedom biphasic analyses, simulations employed the Oakley cluster at Ohio Supercomputer Center (https://www.osc.edu). Each compute node contained 2 Intel Xeon x5650 CPUs. Simulations utilized either 4 or 12 threads and 24 GB of RAM per node.

4. Results

For both loading cases (A and B), the eleven cell representation resulted in wider ranges of predicted cell metrics when compared to the CSC model, especially during the first 20 seconds of the analyses (Figures 2 and 3). Case B resulted in increased transient variability in cell response, as compared to Case A, with 2 to 5 times higher peak values for effective strain, effective stress, maximum shear strain, and mass exchange rates (Figure 2 versus 3). Percent differences typically ranged from 20 to 40% during early loading between the CSC and eleven cell analyses (Figures 4 and 5) and were as high as 60% (Figure 5, blue region). Change in aspect ratio and volumetric strain for Case A loading were the lone exceptions, with differences under 5% (Figure 4). While transient response, likely driven by loading induced fluid flow, was variable, steady-state percent differences (at 100 seconds) between the CSC and eleven cell simulations were less than 4% for all metrics (Figures 2–5).

For the LCSC analyses, when compared to the corresponding EC results, maximum percent differences were less than 4% (Figures 4 and 5, red area). As a function of the entire loading cycle LCSC analyses demonstrated a nearly identical spread as the eleven cell model (Figures 2 and 3) with RMS values (Equation 1) under 0.02. Both percent change as well as

the RMS values between EC and LCSC results indicate the effects of mechanical influence from neighboring cells (Figures 6).

For reference and considering the utilized computational resources (see Methods), computational cost was also documented. The single cell analysis required 3.33 hours of wall clock time (106.5 CPU hours) while the 11 cell case required 3.9 hours (125.17 CPU hours).

5. Discussion

This study successfully highlighted potential differences in transition zone cell mechanics between single and anatomically based eleven cell representations. Concerning aspects of cell health and function, results indicate that for a given point in the cartilage the choice of cell location, as predicted by the anatomically realistic representation of chondrocyte distribution, had a profound effect on transient cell mechanics. Specifically, regarding the choice between a CSC analysis and the random EC distribution, metric specific differences were typically up to 20% yet also as high as 60% (Figures 4 and 5). This was especially evident in the non-symmetric Case B boundary conditions and during the transient response. Regarding the LCSC results, when compared to the corresponding cell in the EC model, normalized RMS values on the order of 0.01 to 0.02 were realized, which captured differences throughout the loading cycle (Figure 6 and Equation 2). While RMS differences were relatively small, the percent difference started small and rose steadily to around 2–4% for all output metrics except mass exchange rate, which was even smaller (Figures 4 and 5). This behavior held up across loading cases A and B. Within the context of this region specific anatomically based cell distribution, realizing the potential for cellular interaction, even if on the order of 4%, highlights an important finding. Current results indicate this observation was a direct result of mechanical cellular interaction, as comparison of the LCSC results with the corresponding cell in the EC simulation offered this possibility.

While the embedded RVE in this biphasic simulation was somewhat shielded from the initial load application, volume averaged cellular strains were highly variable for the 11 cell case, exhibiting both higher and lower strains than the CSC analyses, especially during the transient response (Figures 2 and 3). This somewhat contradicts our previous results, which showed volume averaged cellular strains were lower for an 11 cell versus a single cell RVE [27]. As opposed to the biphasic materials used in this study, hyperelastic material properties representative of instantaneous behavior were adopted in Sibole and Erdemir [27] to predict chondrocyte deformation as a function of joint level loading. The current findings corroborate previous work that highlighted the potential chondroprotective role of the fluid as well as the transient effects of fluid flow though a section of deformed ECM [28], [29]. Another interesting observation, the variability of cell mechanics for the EC and LCSC simulations demonstrated the potential value in quantifying multiple cell level metrics. Gross cellular shape metrics such as aspect ratio are commonly reported in the literature; however, understanding chondrocyte mechanics may be bolstered through the use of additional volume averaged metrics, such as those covered in this study. Still, qualitative comparison with previous work is possible where similar time-dependent behavior was reported for cell level strain values in Guilak and Mow (2000) [25], though that study

modeled unconfined compression. Of note, much longer relaxation times for cell level mechanics have been reported [3], [20]. These studies employed a strain-dependent hydraulic permeability, which would slow relaxation time when the material is compressed. Due to the already high computational burdens of this study, this additional level of realism was not included. Beyond the application of stress relaxation boundary conditions, numerous studies were expanded to include analysis depending on loading frequency [17], [30], which is also possible in an anatomically based multi-cell simulation framework. Such a study could clarify, especially when performed in conjunction with strategies for in-depth sensitivity analysis [25], [31], when elastic based predictions of chondrocyte mechanics are acceptable.

Comparison with previous work should not be limited to simulation based studies, though the difficulty in measuring chondrocyte mechanics could be inferred by the absence of available experimental data, especially if multi-cellular response is considered. Still, comparisons are warranted. One experimental study that utilized unconfined compression tests found engineering strain in a transition zone cell of approximately 0.2 for 10% compressive strain on a cartilage sample [32]. Steady state response in this study yielded a similar result, with an average of 0.25 effective strain across all cells and for both loading cases. While the presented gross mechanical cell level response favorably compares with previous work, as new measurement techniques emerge, the presented study could also help design the setup of new experiments. For instance, if transient chondrocyte mechanical responses for a population could be measured, Case B loading indicates delineation between cells would be more pronounced than Case A. In turn, such experiments would offer ideal data to help establish corresponding modeling capabilities.

Cell placement was found to have a strong influence on the observed transient response of chondrocyte mechanics, as indicated by the variability in cell metrics for the LCSC and EC results (see Results). To test this finding, two additional random cell distributions were evaluated by simply reorienting application of the boundary conditions through the remaining faces of the cartilage mesh, effectively resulting in two additional cell distributions. Results from these post-hoc analyses indicated minimal effect of three separate cases of chondrocyte distributions on the predicted cell mechanics (Figure 7). One exception, a shift was found for change in the aspect ratio, which showed a larger potential range of predicted chondrocyte aspect ratios (Figure 7 versus Figure 3). This finding was found to be driven by the orientation of the mesh in one loading direction, i.e. a mesh effect due to the location of nodes, and the corresponding calculation of the initial cell aspect ratios for this particular direction (Figure 7, see Change in Aspect Ratio (L3:L1)). Similar results were found for Case A loading.

Numerous study assumptions should be considered for further interpretation of our results. Representation of the complexity in the cartilage microstructure, including depth dependent collagen alignment along with cell shape and distribution, was foregone in the interest of a focused study using the transitional region architecture. Unlike the superficial or deep zones, the transitional zone exhibits random collagen fiber alignment and spherical cell shapes, thus justifying the use of simplified geometries and isotropic material models Another consideration is that the anatomically based eleven cell model represents relatively mature

human cartilage and may not apply to developing tissue, which typically exhibits higher cell concentrations [5]. Finally, deterministic representations of material behavior will not capture the influence of known uncertainties [33]. Probabilistic analysis is one approach to address these uncertainties[34] and automated pipelines are necessary to rapidly create desired features at the microstructural level. Such features include parametric definitions of material behavior, cellular shape, orientation and distribution as well as automated post-processing of important cell level mechanical metrics. Related efforts are ongoing [35] and future studies will evaluate complexities such as preferential orientation of collagen fibers, osmotic loading, strain dependent permeability, and non-spherical and non-homogenous chondron distributions, as are found in other regions of the cartilage.

From a technical perspective, multiscale coupling approaches targeting prediction of cell deformations from tissue and/or organ level loading will likely benefit from this investigation while balancing computational demand with accuracy requirements. An embedded construct results in a model with high degrees of freedom, but is attractive due to its coupling between the tissue and micro-scales without abstraction. While acceptable for a test problem, this relatively inefficient setup is not computationally feasible to relate biphasic joint level loading with predictions of location specific chondrocyte mechanics [27]. For the presented biphasic simulation, RVE model convergence was one consideration that drove the choice to develop an embedded construct. Likely more beneficial, however, is that direct coupling (through shared nodes) of the RVE and the surrounding tissue ensures mechanical consistency between the scales. Ongoing efforts, which consider concurrent multiscale coupling of cartilage (macrostructural) and chondrocyte (microstructural) mechanics, will benefit from a problem able to evaluate scale coupling assumptions, as presented here. Our recent work indicates the possibility to couple simulation of macrostructural cartilage behavior to chondrocyte mechanics with second order passing schemes [23], but questions remain on the applicability to other cartilage regions and cell densities.

The specific goals of this study coincide with the long term vision toward development of physically meaningful body level simulations focused on the underlying cell vitality and mechanobiology. It is well established that cell mechanics depend on their surrounding medium [4], and that cellular processes can be regulated by mechanical input [1]. This study illustrates that an anatomical representation of cell distribution may be necessary, especially if one is interested in anatomically based representation of a chondrocyte population, which includes the potential for cellular interactions. Across metrics of cell mechanics for the specialized case of transitional zone of cartilage, the effect of neighboring cells was found to influence steady-state cell mechanics on the order of 4%. At the chosen level of complexity, this study realized marked differences in the transient cellular strains and fluid flow behavior between CSC and EC models. That stated, results from both the EC the LCSC simulations indicate the importance of cell location and the potential for cellular mechanical interaction. These findings address the efficacy of predicting cellular response from a homogenous macrostructural model (e.g. transitional zone cartilage), where predictions of cell mechanics may benefit from an explicit representation of cell distribution [36]. While cell density and tissue complexity may play a role in this regard, it is also recognized that homogeneous constitutive models at the tissue scale, representative of underlying cell distribution and

mechanics, may also be feasible if accurate data passing schemes are adopted [23]. From a functional perspective, implications also include, among others, development of an evaluation tool able to address mechanobiological aspects of chondrocyte mechanics, all within the context of tissue-scale loading.

Acknowledgments

This study was funded by the National Institute of Biomedical Imaging and Bioengineering, National Institutes of Health (R01EB009643: Erdemir, Principal Investigator). Computing resources from Ohio Supercomputer Center are greatly appreciated.

References

1. Grodzinsky AJ, Levenston ME, Jin M, Frank EH. Cartilage tissue remodeling in response to mechanical forces. Annu Rev Biomed Eng. 2000; 2:691–713. [PubMed: 11701528]
2. Chen AC, Bae WC, Schinagl RM, Sah RL. Depth- and strain-dependent mechanical and electromechanical properties of full-thickness bovine articular cartilage in confined compression. J Biomech. Jan; 2001 34(1):1–12. [PubMed: 11425068]
3. Han SK, Federico S, Herzog W. A depth-dependent model of the pericellular microenvironment of chondrocytes in articular cartilage. Comput Methods Biomech Biomed Engin. Jul; 2011 14(7):657–664. [PubMed: 20665295]
4. Urban JP. Present perspectives on cartilage and chondrocyte mechanobiology. Biorheology. 2000; 37(1–2):185–190. [PubMed: 10912191]
5. Quinn TM, Hunziker EB, Häuselmann HJ. Variation of cell and matrix morphologies in articular cartilage among locations in the adult human knee. Osteoarthr Cartil. Aug; 2005 13(8):672–678. [PubMed: 15970445]
6. Helminen HJ, et al. Regular joint loading in youth assists in the establishment and strengthening of the collagen network of articular cartilage and contributes to the prevention of osteoarthrosis later in life: a hypothesis. J Bone Miner Metab. 2000; 18(5):245–257. [PubMed: 10959613]
7. Halloran JP, et al. Multiscale Mechanics of Articular Cartilage: Potentials and Challenges of Coupling Musculoskeletal, Joint, and Microscale Computational Models. Annals of biomedical engineering. May.2012
8. Han SK, Madden R, Abusara Z, Herzog W. In situ chondrocyte viscoelasticity. J Biomech. Sep; 2012 45(14):2450–2456. [PubMed: 22884037]
9. Guilak F. Volume and surface area measurement of viable chondrocytes in situ using geometric modelling of serial confocal sections. J Microsc. Mar; 1994 173(Pt 3):245–256. [PubMed: 8189447]
10. Moo EK, et al. Extracellular matrix integrity affects the mechanical behaviour of in-situ chondrocytes under compression. J Biomech. Mar; 2014 47(5):1004–1013. [PubMed: 24480705]
11. Abusara Z, Seerattan R, Leumann A, Thompson R, Herzog W. A novel method for determining articular cartilage chondrocyte mechanics in vivo. J Biomech. Mar; 2011 44(5):930–934. [PubMed: 21145552]
12. Madden RMJ, Han SK, Herzog W. The effect of compressive loading magnitude on in situ chondrocyte calcium signaling. Biomech Model Mechanobiol. Jan; 2015 14(1):135–142. [PubMed: 24853775]
13. Zelenski NA, et al. Type VI Collagen Regulates Pericellular Matrix Properties, Chondrocyte Swelling, and Mechanotransduction in Mouse Articular Cartilage. Arthritis & Rheumatology (Hoboken NJ). May; 2015 67(5):1286–1294.
14. Stolz M, Raiteri R, Daniels AU, VanLandingham MR, Baschong W, Aebi U. Dynamic elastic modulus of porcine articular cartilage determined at two different levels of tissue organization by indentation-type atomic force microscopy. Biophys J. May; 2004 86(5):3269–3283. [PubMed: 15111440]

15. Ofek G, Dowling EP, Raphael RM, McGarry JP, Athanasiou KA. Biomechanics of single chondrocytes under direct shear. Biomechanics and Modeling in Mechanobiology. 2010; 9(2):153–162. [PubMed: 19644718]
16. Guilak, F., Hung, CT. Physical Regulation of Cartilage Metabolism. In: Mow, VC., Huiskes, R., editors. Basic Orthopaedic Biomechanics and Mechanobiology. Philadelphia: Lippincott Williams & Wilkins; 2005. p. 259-300.
17. Kim E, Guilak F, Haider MA. The dynamic mechanical environment of the chondrocyte: a biphasic finite element model of cell-matrix interactions under cyclic compressive loading. J Biomech Eng. Dec.2008 130(6):061009. [PubMed: 19045538]
18. Federico S, Grillo A, La Rosa G, Giaquinta G, Herzog W. A transversely isotropic, transversely homogeneous microstructural-statistical model of articular cartilage. J Biomech. Oct; 2005 38(10): 2008–2018. [PubMed: 16084201]
19. Korhonen RK, Han SK, Herzog W. Osmotic loading of articular cartilage modulates cell deformations along primary collagen fibril directions. J Biomech. Mar; 2010 43(4):783–787. [PubMed: 19892355]
20. Korhonen RK, Herzog W. Depth-dependent analysis of the role of collagen fibrils, fixed charges and fluid in the pericellular matrix of articular cartilage on chondrocyte mechanics. J Biomech. 2008; 41(2):480–485. [PubMed: 17936762]
21. Mow VC, Kuei SC, Lai WM, Armstrong CG. Biphasic creep and stress relaxation of articular cartilage in compression? Theory and experiments. J Biomech Eng. Feb; 1980 102(1):73–84. [PubMed: 7382457]
22. Federico S, Grillo A, La Rosa G, Giaquinta G, Herzog W. A transversely isotropic, transversely homogeneous microstructural-statistical model of articular cartilage. J Biomech. Oct; 2005 38(10): 2008–2018. [PubMed: 16084201]
23. Sibole SC, Maas S, Halloran JP, Weiss JA, Erdemir A. Evaluation of a post-processing approach for multiscale analysis of biphasic mechanics of chondrocytes. Comput Methods Biomech Biomed Engin. Oct; 2013 16(10):1112–1126. [PubMed: 23809004]
24. Bennetts CJ, Sibole S, Erdemir A. Automated generation of tissue-specific three-dimensional finite element meshes containing ellipsoidal cellular inclusions. Comput Methods Biomech Biomed Engin. 2015; 18(12):1293–1304. [PubMed: 24708340]
25. Guilak F, Mow VC. The mechanical environment of the chondrocyte: a biphasic finite element model of cell-matrix interactions in articular cartilage. J Biomech. Dec; 2000 33(12):1663–1673. [PubMed: 11006391]
26. Maas SA, Ellis BJ, Ateshian GA, Weiss JA. FEBio: Finite Elements for Biomechanics. J Biomech Eng. Jan.2012 134(1):011005. [PubMed: 22482660]
27. Sibole SC, Erdemir A. Chondrocyte deformations as a function of tibiofemoral joint loading predicted by a generalized high-throughput pipeline of multi-scale simulations. PLoS ONE. 2012; 7(5):e37538. [PubMed: 22649535]
28. Clark AL, Votta BJ, Kumar S, Liedtke W, Guilak F. Chondroprotective role of the osmotically sensitive ion channel transient receptor potential vanilloid 4: age- and sex-dependent progression of osteoarthritis in Trpv4-deficient mice. Arthritis Rheum. Oct; 2010 62(10):2973–2983. [PubMed: 20583100]
29. Alexopoulos LG, Setton LA, Guilak F. The biomechanical role of the chondrocyte pericellular matrix in articular cartilage. Acta Biomater. May; 2005 1(3):317–325. [PubMed: 16701810]
30. Kim Y, Bonassar L, Grodzinsky A. The Role of Cartilage Streaming Potential, Fluid-Flow and Pressure in the Stimulatin of Chondrocyte Biosynthesis During Dynamic Compression. J Biomech. Sep; 1995 28(9):1055–1066. [PubMed: 7559675]
31. Laz PJ, Pal S, Halloran JP, Petrella AJ, Rullkoetter PJ. Probabilistic finite element prediction of knee wear simulator mechanics. J Biomech. 2006; 39(12):2303–2310. [PubMed: 16185700]
32. Choi JB, et al. Zonal changes in the three-dimensional morphology of the chondron under compression: the relationship among cellular, pericellular, and extracellular deformation in articular cartilage. J Biomech. 2007; 40(12):2596–2603. [PubMed: 17397851]

33. Korhonen RK, Julkunen P, Rieppo J, Lappalainen R, Konttinen YT, Jurvelin JS. Collagen network of articular cartilage modulates fluid flow and mechanical stresses in chondrocyte. Biomech Model Mechanobiol. Jun; 2006 5(2–3):150–159. [PubMed: 16506019]

34. Haldar, A., Mahadevan, S. Probability, reliability, and statistical methods in engineering design. John Wiley; 2000.

35. Erdemir A, Bennetts C, Davis S, Reddy A, Sibole S. Multiscale cartilage biomechanics: technical challenges in realizing a high-throughput modelling and simulation workflow. Interface Focus. Apr.2015 5(2):20140081. [PubMed: 25844153]

36. Breuls RGM, Sengers BG, Oomens CWJ, Bouten CVC, Baaijens FPT. Predicting local cell deformations in engineered tissue constructs: a multilevel finite element approach. J Biomech Eng. Apr; 2002 124(2):198–207. [PubMed: 12002129]

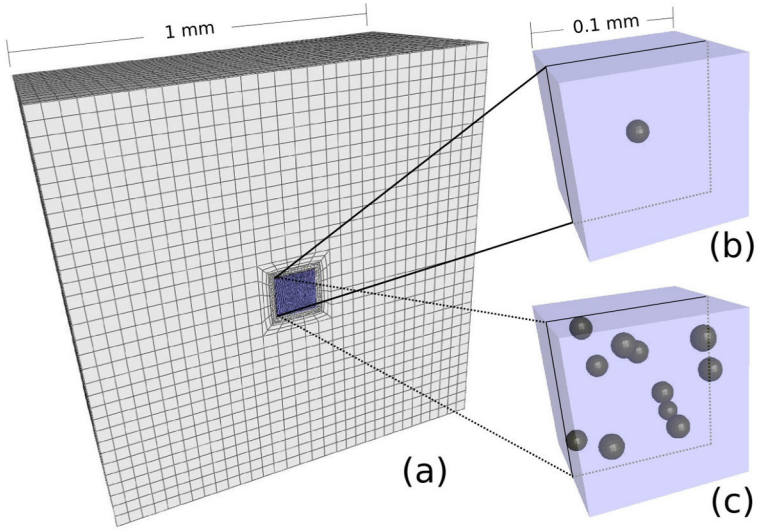

Figure 1.
1x1x1 mm^3 finite element mesh construct with the embedded 100 x 100 x 100 μm^3 representative volume element (RVE) cell-scale models. Close-ups of the (b) single cell and (c) eleven cell model are highlighted. Note the spheres in subplots b and c represent the chondron (chondrocyte plus the pericellular matrix).

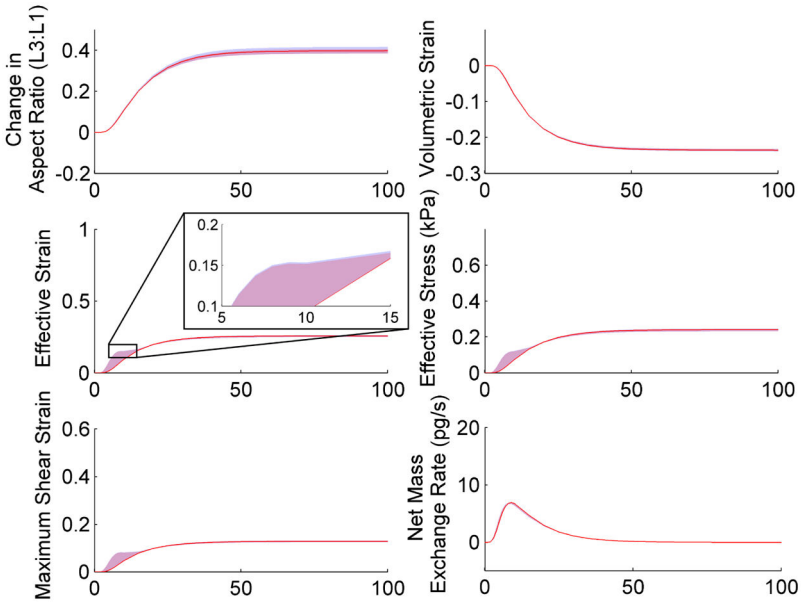

Figure 2.

Cell results as a function of time for Case A boundary conditions (10% strain stress-relaxation, confined compression, free draining top and bottom surfaces). Centered single cell (CSC) results are represented by the solid red line while the ranges of eleven cell (EC) and location corrected single cell (LCSC) results are shown in the blue and red shaded regions, respectively. Note the zoomed in view for maximum shear strain (bottom left) highlights the bounds for both the eleven cell and LCSC results. Effectively, the bounds for the EC and the LCSC were coincident. This behavior was typical across all metrics.

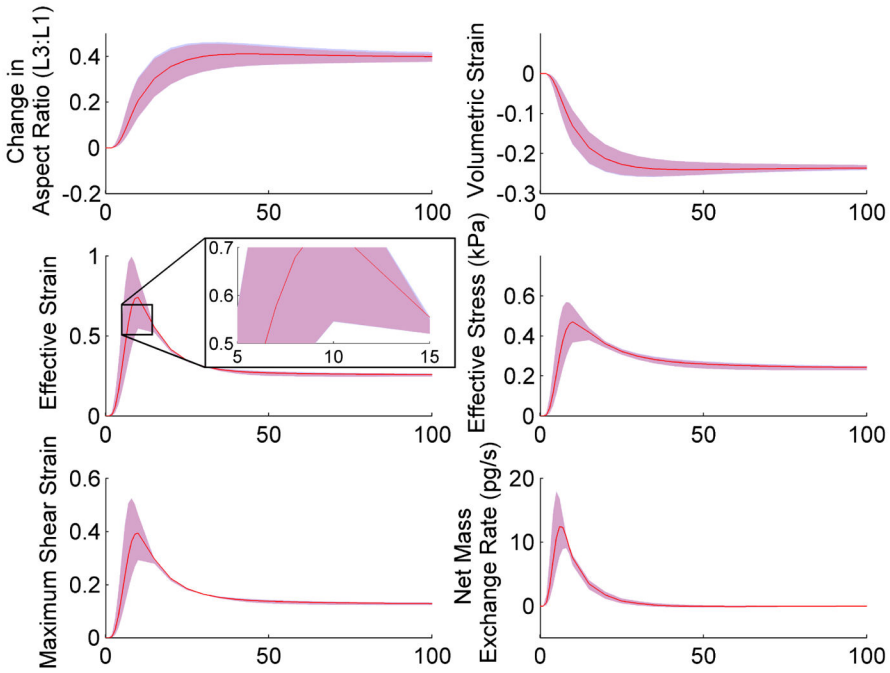

Figure 3.

Cell results as a function of time for Case B boundary conditions (10% strain stress-relaxation, confined compression, free draining top surface only). Centered single cell (CSC) results are represented by the solid red line while the ranges of eleven cell (EC) and location corrected single cell (LCSC) results are shown in the blue and red shaded regions, respectively. Note the zoomed in view for maximum shear strain (bottom left) highlights the bounds for both the EC and LCSC results. This behavior was typical across all metrics.

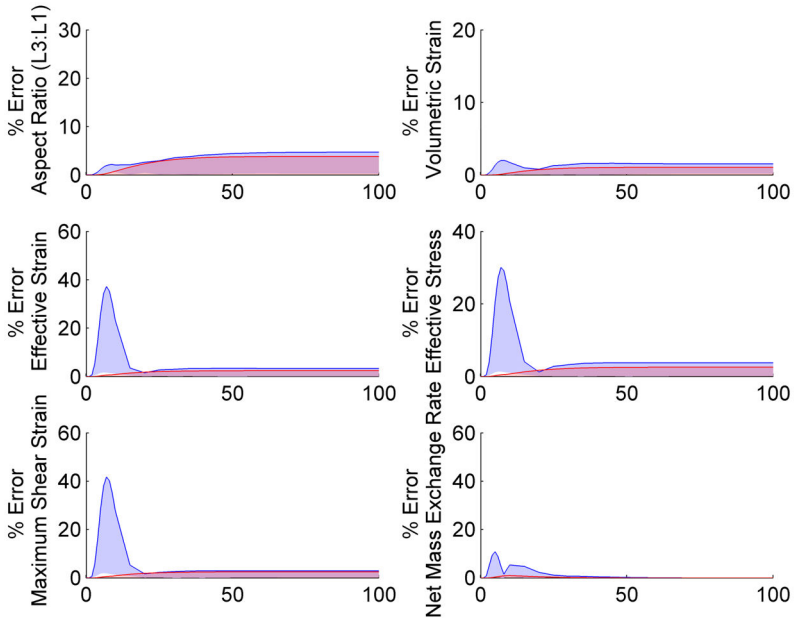

Figure 4.

Percent difference throughout the Case A loading history between the centered single cell (CSC) and each of the eleven cells (blue region) as well as the location corrected single cells (LCSC) and its corresponding cell in the eleven cell (EC) simulation (red region). Each metric was plotted individually and correspond to the metrics presented in Figures 2 and 3.

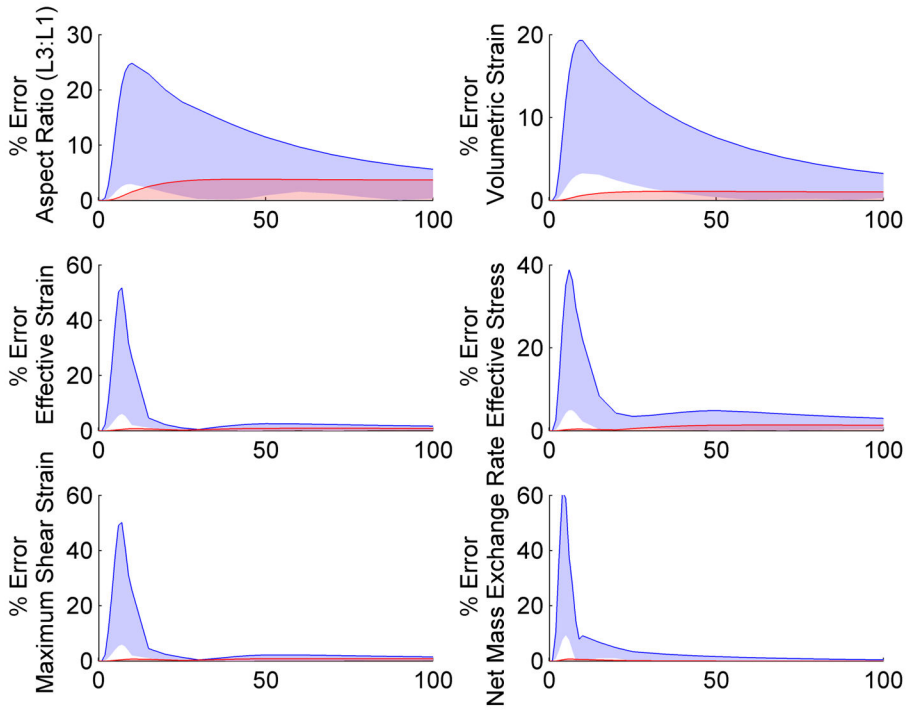

Figure 5.

Percent difference throughout the Case B loading history between the centered single cell (CSC) and each of the eleven cells (EC, blue region) as well as the location corrected single cells (LCSC) and its corresponding cell in the EC simulation (red region). Each metric was plotted individually and correspond to the metrics presented in Figures 2 and 3.

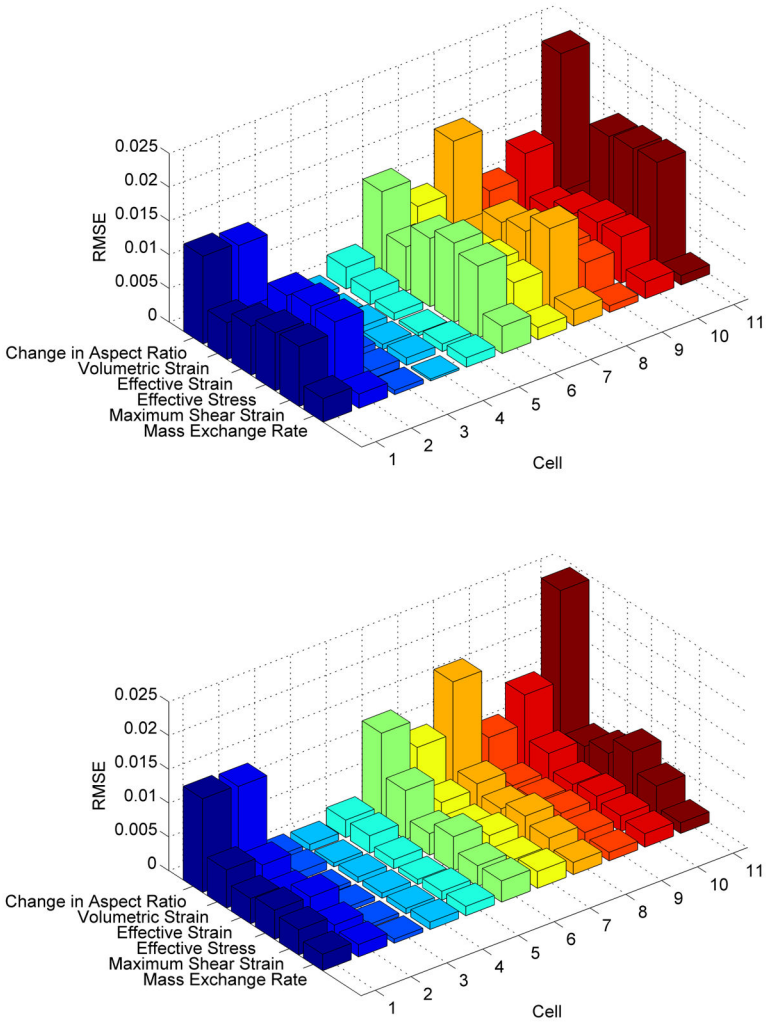

Figure 6.

RMS values (Equation 2) for all cells and metrics between the eleven cell (EC) and location corrected single cell analyses (LCSC) for both Case A (top) and Case B (bottom) boundary conditions. Including all eleven cells shows the cell specific results as well as the visual comparison between all simulations. Note that cell number 11, in terms of physical location, was closest to the single cell model.

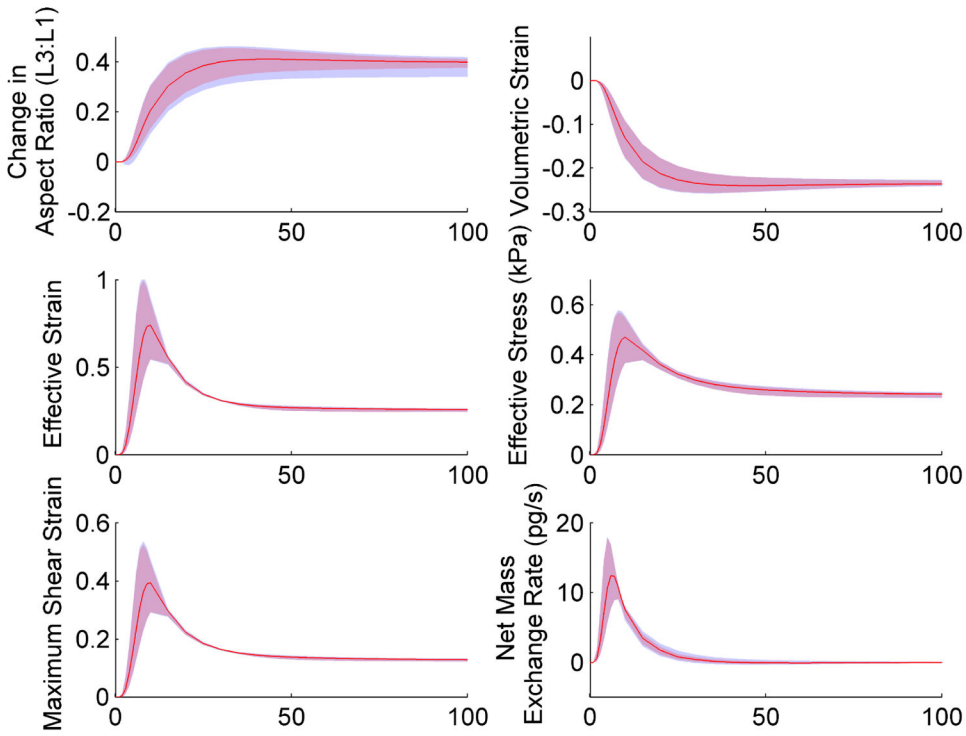

Figure 7.

Cell results for three random cell models, as achieved by changing the loading direction for the presented eleven cell (EC) model (Figure 1), as a function of time for Case B boundary conditions.